International Journal of Mechanical, Industrial and Aerospace Sciences
ISSN: 2517-9950
Vol:14, No:9, 2020

Dynamic Stall Characterization of Low Reynolds Airfoil in Mars and Titan's Atmosphere

Vatasta Koul, Vaibhav Sharma, Ayush Gupta, Rajesh Yadav

***Abstract*—**Exploratory missions to Mars and Titan have increased recently with various endeavors to find an alternate home to humankind. The use of surface rovers has its limitations due to rugged and uneven surfaces of these planetary bodies. The use of aerial robots requires the complete aerodynamic characterization of these vehicles in the atmospheric conditions of these planetary bodies. The dynamic stall phenomenon is extremely important for rotary wings performance under low Reynolds number that can be encountered in Martian and Titan's atmosphere. The current research focuses on the aerodynamic characterization and exploration of the dynamic stall phenomenon of two different airfoils viz. E387 and Selig-Donovan7003 in Martian and Titan's atmosphere at low Reynolds numbers of 10000 and 50000. The two-dimensional numerical simulations are conducted using commercially available finite volume solver with multi-species non-reacting mixture of gases as the working fluid. The k-epsilon (k-ε) turbulence model is used to capture the unsteady flow separation and the effect of turbulence. The dynamic characteristics are studied at a fixed different constant rotational extreme of angles of attack. This study of airfoils at different low Reynolds number and atmospheric conditions on Mars and Titan will be resulting in defining the aerodynamic characteristics of these airfoils for unmanned aerial missions for outer space exploration.

***Keywords*—**Aerodynamic, dynamic stall, low Reynolds, Mars, Titan.

I. Introduction

AIRFOIL is a type of body used in aerodynamic application as it produced aerodynamic forces when a fluid is allowed to flow over it. There are two types of the forces produced when a fluid is allowed to flow over an airfoil; the horizontal force which is called as drag and a vertical force which is called as lift. These are used in various aerodynamic applications and even in a turbine blade they prefer the airfoil shaped blade. These come in various shapes and each has very unique advantages. The straight line joining the leading edge and trailing edge of the airfoil is called chord length. Further, the line joining the leading edge and trailing edge following the curvature of the airfoil exactly at the centre of the airfoil is called the Camber length. For a symmetric airfoil both Camber length and chord length are the same (Fig. 1) but for non-symmetrical airfoil they will be different (Fig. 1). The airfoil works on a Bernoulli's principle. For a symmetric airfoil at zero angle of attack there will not be any lift as the flow passing on the top surface will be same as the bottom surface but when the angle of attack increases the velocity of the top surface of the airfoil also increases, this increase in the velocity in turn reduces the pressure on the top surface of the flow generating a pressure difference on top and bottom edge of the airfoil due to which the lift will increase. But the case of non-symmetrical airfoil is different; these can produce lift at 0º AOA due to particular shape of the airfoil. The velocity gradient on the top of the airfoil is more than the bottom edge creating a pressure difference between both edges. The increase in AOA of the airfoil also creates some complications such as stall and it is cased due to the flow separation.

Stall is a phenomenon occurred when the AOA exceeds a certain limit the lift starts to decrease. This happens due to the increase in angle of attack due to which the fluid on top surface of the airfoil moves faster resulting in a lower pressure on top of the airfoil. This low pressure leads to an adverse pressure gradient (or positive pressure gradient) on top of airfoil and due to which flow separates. As AOA increases, the adverse pressure gradient increases resulting in slowing down the boundary layer and creating a negative velocity gradient. Further increase in AOA leads to separation of the flow near the leading edge and the bubble is formed which is called as leading edge vortex (LEV).

II. Dynamic Stall

An airfoil that reports an unsteady increase in the occurrence which incorporates it past its static stall perspective is understood to increase. This increase in the lift is without any detectable trade within the lift-curve slope [7]. This has also been found on helicopter rotors in which changes in angle-of-attack are predominant [8]. Upon further analysis on the helicopter, it is observed that the lift generated extra on the rotors of the helicopters could be explained if lift on the blade is more than that predicted by steady flow which is when the helicopter blades are moving in the direction opposite to that of the flight [6]. Although dependent on the rate and amplitude of the oscillation, it is commonly observed that because the airfoil keeps pitching upward, a stage is reached wherein a surge in the elevate force and a negative roll-off in the pitching moment occurs. Simultaneously, the vortex can be seen to develop and be shed from the leading-edge region. As the flow moves over the rear its size grows and negative moments are brought about with sudden loss in the lift [5].

During the next portion of the cycle the airfoil will be in deep-stall and under an extensive region of separated flow [1]. In general terms this describes the familiar features of

Vatasta Koul, Vaibhav Sharma, Ayush Gupta are with the Department of Aerospace at University of Petroleum and Energy Studies, Dehradun 248007, Uttarakhand, India (e-mail: vatastakoul@gmail.com).
Rajesh Yadav is Assistant Professor, Dehradun, Uttarakhand, 248007.

dynamic stall as observed in two-dimensional flow experiments; however, to better understand the stall phenomenon it is necessary to examine in greater detail. The first distinguishing difference between the static and dynamic stall behaviour of an airfoil is that the break in the lift and moment curves no longer occur at the same time, nor for the same reason. Moment stall, which is due to the growth and initial shedding of the vortex in the dynamic case, can be defined in general as the point where the pressure distribution is altered sufficiently to produce a noticeable negative divergence in the pitching moment. Lift stall, which is a necessary consequence of vortex shedding in most dynamic cases, can in general be defined as the point where the boundary layer has sufficiently separated so that the resulting pressure distribution no longer yields an increase in lift with further increases in incidence.

A. Light Dynamic Stall

This type of dynamic stall occurs when you pitch the airfoil to a particular angle of attack. The properties of this kind of stall are almost similar to the static stall condition, such as decrease in the lift and increase in the drag, since the dynamic stall is an unsteady phenomenon.

B. Deep Dynamic Stall

The deep dynamic stall occurs when we oscillate the airfoil at higher angle of attack than the light dynamic stall. The vortex shedding phenomenon dominates in this type of the stall. The vortex formed at the leading edge move along the top surface of the airfoil and leads to increase of Cl, Cd values; it will be interesting to see how these phenomena vary when we allowed them in Martian atmosphere.

The dynamic stall is more difficult to analyze because it depends on various factors such as pitching frequency, pitching angle, Reynolds Number and geometry of airfoil.

C. Martian and Titan Atmospheres

The mars atmosphere majorly consists of carbon dioxide (around 95%), nitrogen (2.6%), argon (1.9%), traces of oxygen and water vapour. The pressure on the mars is very less compared to the earth atmosphere which changes from location to location around 600 Pa, density of the air is also less somewhere around 0.012 kg/m^3, viscosity is 1.14×10^5 kg/ms, the average temperature of mars atmosphere is 260K and the speed of the sound is 256 m/s, the gravitational force is also less in the mars atmosphere 3.11 m/s^2 [2]. The surface of the mars is at an even an altitude of the surface is high from place to place, so we need a UAV such that it can generate a high lift within small time so that the object can move from lower altitude to higher altitude. Recent technological advancement in the aerospace industry and in compact electronics led to the discovery of micro air vehicle (MAV), unmanned air vehicles and mars exploration vehicles (MEV). On the other hand, Titan provides a good analogue as a natural laboratory in which chemical and physical processes can be studied on a planetary scale and help us understand early chemical evolution in the primordial atmosphere on Earth. Titan has a thick and extended atmosphere mainly composed of N_2 (97%) and CH4 (1.5%), with the surface temperature of T = 94K and surface pressure = 1.5 bar. It has an intense and complex chemistry {C, H, N, O} leading to different hydrocarbons, nitriles and oxygen species [4].

In Titan's conditions, CH_4 and C_2H_6 can condense and produce clouds, haze and surface is found to be liquid. The climate is found to be of exotic nature having different hydrocarbon cycles analogous to Earth's hydrological cycle producing clouds, rain, lakes etc. The surface looks familiar to that of Earth but with different material and shaped by weather, with lakes/seas, dunes, channels.

III. Methodology

The purpose of the investigation is to quantify that the dynamic stall phenomenon is an extremely important phenomenon for rotary wings' performance under low Reynolds number that can be encountered in Martian and Titan's atmosphere. The current research focuses on the aerodynamic characterization and exploration of the dynamic stall phenomenon of three low Reynolds number airfoils viz. E387 and SD7003, in Martian and Titan's atmosphere at low Reynolds numbers of 10000 and 50000. The k-epsilon (k-ε) turbulence model is used to capture the unsteady flow separation and the effect of turbulence. The dynamic characteristics are studied at a fixed different constant rotational extreme of angles of attack.

Navier-Stokes Equations:

Continuity:

$$\frac{\partial \rho}{\partial t} = -\left[\frac{\partial(\rho u)}{\partial x} + \frac{\partial(\rho v)}{\partial y} + \frac{\partial(\rho w)}{\partial z}\right] \quad (1)$$

X Momentum:

$$\frac{\partial u}{\partial t} = -u\frac{\partial u}{\partial x} - v\frac{\partial u}{\partial y} - w\frac{\partial u}{\partial z} + \frac{1}{\rho}\left[-\frac{\partial p}{\partial x} + \frac{\partial \tau_{xx}}{\partial x} + \frac{\partial \tau_{yx}}{\partial y} + \frac{\partial \tau_{zx}}{\partial z}\right] \quad (2)$$

Y Momentum:

$$\frac{\partial v}{\partial t} = -u\frac{\partial v}{\partial x} - v\frac{\partial v}{\partial y} - w\frac{\partial v}{\partial z} + \frac{1}{\rho}\left[-\frac{\partial p}{\partial y} + \frac{\partial \tau_{xy}}{\partial x} + \frac{\partial \tau_{yy}}{\partial y} + \frac{\partial \tau_{zy}}{\partial z}\right] \quad (3)$$

Z Momentum:

$$\frac{\partial w}{\partial t} = -u\frac{\partial w}{\partial x} - v\frac{\partial w}{\partial y} - w\frac{\partial w}{\partial z} + \frac{1}{\rho}\left[-\frac{\partial p}{\partial z} + \frac{\partial \tau_{xz}}{\partial x} + \frac{\partial \tau_{yz}}{\partial y} + \frac{\partial \tau_{zz}}{\partial z}\right] \quad (4)$$

Energy:

$$\frac{\partial(e+\frac{V^2}{2})}{\partial t} = -u\frac{\partial\left(e+\frac{V^2}{2}\right)}{\partial x} - v\frac{\partial\left(e+\frac{V^2}{2}\right)}{\partial y} - w\frac{\partial\left(e+\frac{V^2}{2}\right)}{\partial z} + q + \frac{1}{\rho}\left[\frac{\partial}{\partial x}\left(k\frac{\partial T}{\partial x}\right) + \frac{\partial}{\partial y}\left(k\frac{\partial T}{\partial y}\right) + \frac{\partial}{\partial z}\left(k\frac{\partial T}{\partial z}\right) - \frac{\partial(pu)}{\partial x} - \frac{\partial(pv)}{\partial y} - \frac{\partial(pw)}{\partial z} + \frac{\partial(u\tau_{xx})}{\partial x} + \frac{\partial(u\tau_{yx})}{\partial y} + \frac{\partial(u\tau_{zx})}{\partial z} + \frac{\partial(v\tau_{xy})}{\partial x} + \frac{\partial(v\tau_{yy})}{\partial y} + \frac{\partial(v\tau_{yz})}{\partial z} + \frac{\partial(w\tau_{xz})}{\partial x} + \frac{\partial(w\tau_{yz})}{\partial y} + \frac{\partial(w\tau_{zz})}{\partial z}\right] \quad (5)$$

These equations have been written with the time derivatives on the left-hand side and all spatial derivatives on the right-hand side. This is the form suitable to the time dependent solution of the equation. These equations are partial

differential equations that have a mathematically elliptic behavior that is, on a physical basis they treat flow field information and flow distribution that can travel throughout the flow field, in both upstream and downstream directions [3].

Three different airfoils are studied: E387 airfoil and SD7003 airfoil. Each was pitch oscillating about one-fourth chord location to the sinusoidal mode.

$$\alpha = 30.\sin(2\pi.\ f.t) \tag{6}$$

The frequency is obtained by reduced frequency k [1]:

$$k = \frac{\pi.f.c}{U_\infty} \tag{7}$$

There will be three cases about the reduced frequency: 0.5 and 0.25. U_∞ is determined by the Reynold's number Re:

$$Re = \frac{\rho.c.U_\infty}{\mu} \tag{8}$$

Again, three cases are studied about Reynold's number: 10000 and 50000. As the turbulence solver, the k-ε equation is used. The k-ε equation has various unmeasurable and unknown terms. For a substantially more functional methodology, the standard k-ε turbulence model is utilized which depends on our best understanding of the significant procedures, along these lines limiting unknowns and introducing a lot of conditions that can be applied to a large number of turbulent applications.

For turbulent Kinetic Energy k:

$$\frac{\partial(\rho k)}{\partial t} + \frac{\partial(\rho k u_i)}{\partial x_i} = \frac{\partial}{\partial x_j}\left[\frac{\mu_t}{\sigma_k}\frac{\partial k}{\partial x_j}\right] + 2\mu_t E_{ij}E_{ij} - \rho\varepsilon \tag{9}$$

For dissipation ε:

$$\frac{\partial(\rho\varepsilon)}{\partial t} + \frac{\partial(\rho\varepsilon u_i)}{\partial x_i} = \frac{\partial}{\partial x_j}\left[\frac{\mu_t}{\sigma_\varepsilon}\frac{\partial \varepsilon}{\partial x_j}\right] + C_{l\varepsilon}\frac{\varepsilon}{k}2\mu_t E_{ij}E_{ij} - C_{2\varepsilon}\rho\frac{\varepsilon^2}{k} \tag{10}$$

where u_i represents velocity component of rate of deformation, E_{ij} represents component of rate of deformation, μ_t represents viscosity

$$\mu_t = \rho C_\mu \frac{k^2}{\varepsilon} \tag{11}$$

A 2D-grid layout has been generated with the CATIA CAD application from ANSYS R2019. The geometry is modelled as shown on Fig. 1. The coordinates of the airfoils were recovered from the site [9]. The coordinates were downloaded and directly imported to plot the airfoil. The domain is composed by a half circle with a diameter of 2800 mm in front of the airfoil and a rectangle of 2800 mm in the back. The airfoil had a chord of 200 mm. It possesses 3 areas namely far-field domain, rotating domain 600 mm around the airfoil and one downstream domain, with a height of 300 mm.

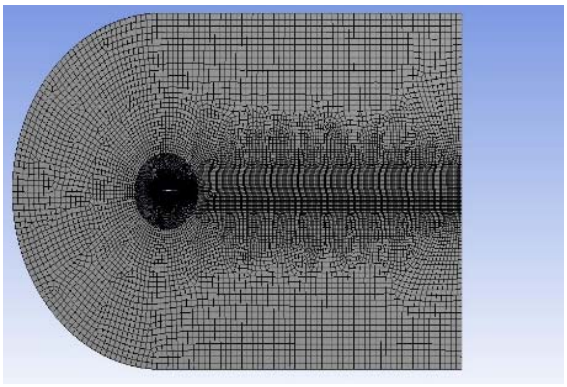

Fig. 1 Two-Dimensional Numerical Mesh

Mesh has been generated using ANSYS Meshing tool with all quadrilateral dominance for each body. A body sizing was used for each body to change the scale of elements. The far-field domain is composed by 0.05 m long elements. The downstream domain is composed by 0.0135 m long elements. The rotating domain is composed by 0.009 m long elements with 133823 elements and an inflation of 10 layers around the airfoil.

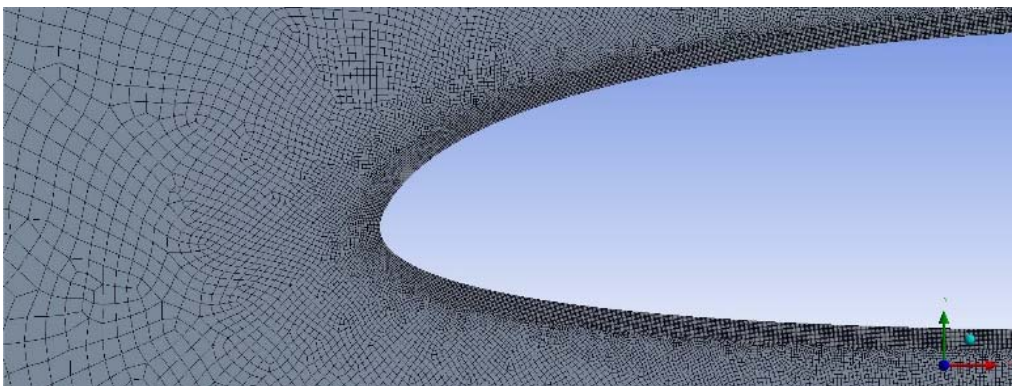

Fig. 2 Inflation layer over the airfoil

TABLE I
DIFFERENT ROTATIONAL FREQUENCY (K) AND VELOCITY VALUES

Atmosphere	k (rad/s)	Re	U (m/s)
Mars	0.25	10000	41.075
		50000	271.79
	0.5	10000	41.075
		50000	271.79
Titan	0.25	10000	6.019
		50000	30.093
	0.5	10000	6.019
		50000	30.093

IV. RESULTS AND DISCUSSIONS

The results can be seen from the curves of coefficient of lift (C_l) as a function of angle of attack (α) obtained from the simulations.

A. E387 in Martian and Titan Atmosphere

It can been observed in the first case that at k = 0.25 rad/s, close similarities can be seen in the behaviors of lift coefficient at the same reduced frequency on both Mars and Titan. As we can see from the velocity contour in Figs. 7 (a)-(c), during the pre-stall condition, there is a higher velocity at the upper surface thus resulting in lower pressure. At the stall condition on Titan at Re = 50000 and k = 0.25 rad/s we can see the flow separation region over the surface of the airfoil where the stalling angle is around 16.62 degrees. In the post stall condition, the wake region is formed.

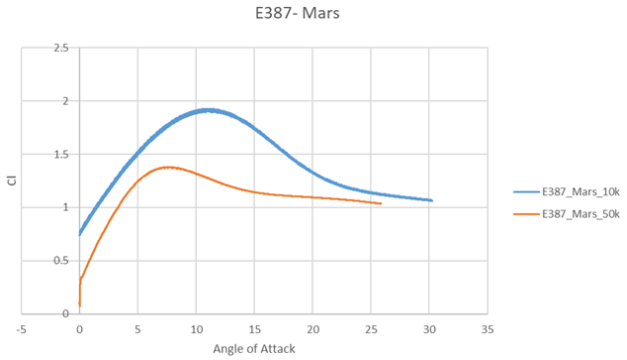

Fig. 3 C_l vs α for E387 on Mars at Re = 10000 and Re = 50000 with k = 0.5 rad/s

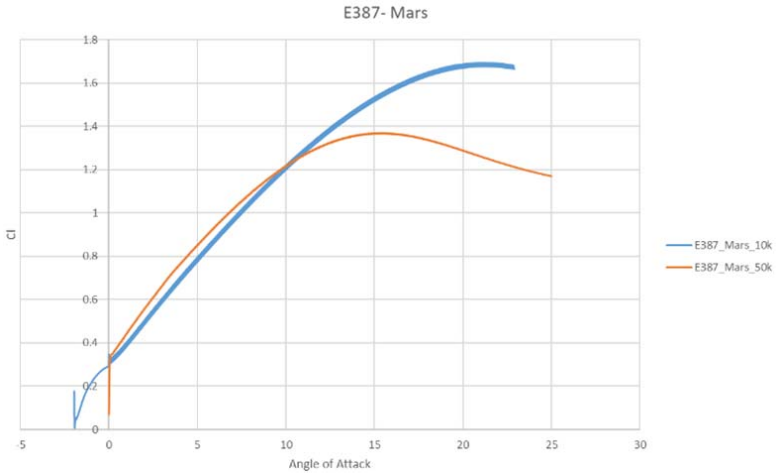

Fig. 4 C_l vs α for E387 on Mars at Re = 10000 and Re = 50000 with k = 0.25 rad/s

The stall angles at the two reduced frequency k = 0.25 rad/s and k = 0.50 and at two different low Reynolds number of 10000 and 50000 on Mars can be seen in Table III. It can be interpreted from the table that the stall angle is delayed in case of low Reynolds number of 10000.

The stall angles at the two reduced frequency and at the two different low Reynolds numbers of 10000 and 50000 on Mars can be seen in Table III. The stall in the Titan atmosphere is almost same for both Re = 10000 and Re = 50000.

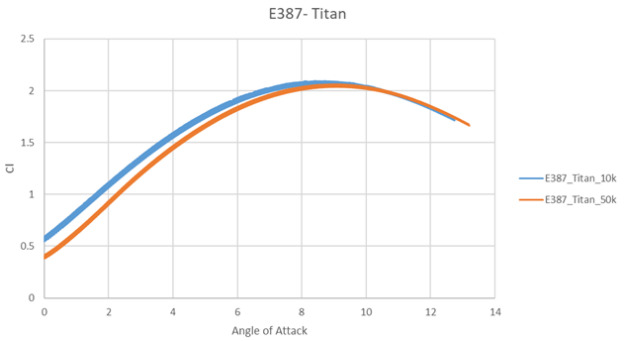

Fig. 5 C_l vs α for E387 on Titan at Re = 10000 and Re = 50000 with k = 0.5 rad/s

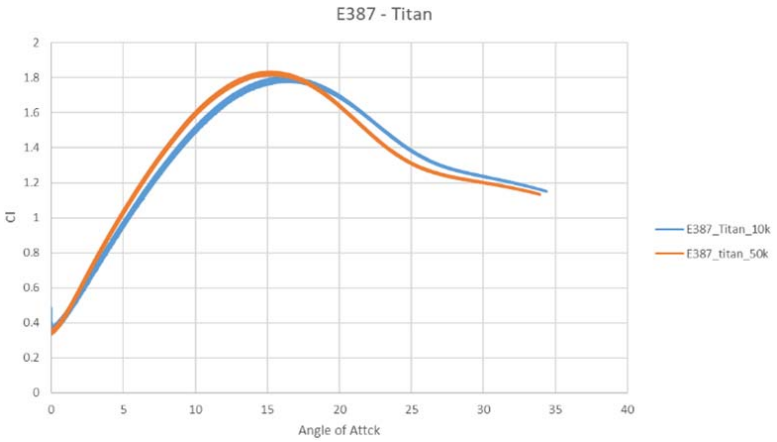

Fig. 6 C_l vs α for E387 on Titan at Re = 10000 and Re = 50000 with k = 0.25 rad/s

TABLE II
STALL ANGLES ON TITAN

E387_Titan		
k	Re	Stall angle
0.25	10000	17.67
	50000	16.62
0.5	10000	8.4
	50000	10.57

TABLE III
STALL ANGLES ON MARS

E387_Mars		
k	Re	Stall angle
0.25	10000	20.16
	50000	17.36
0.5	10000	12.41
	50000	9.23

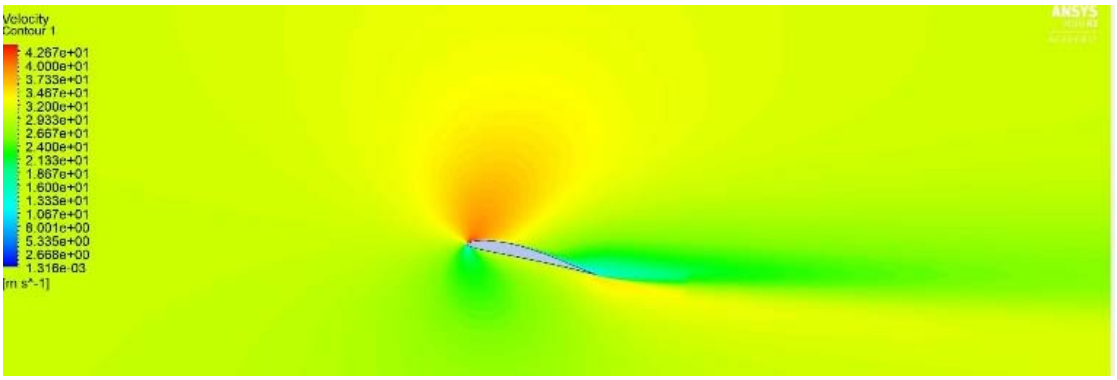

Fig. 7 (a) Velocity Contour of E387 in pre-stall condition

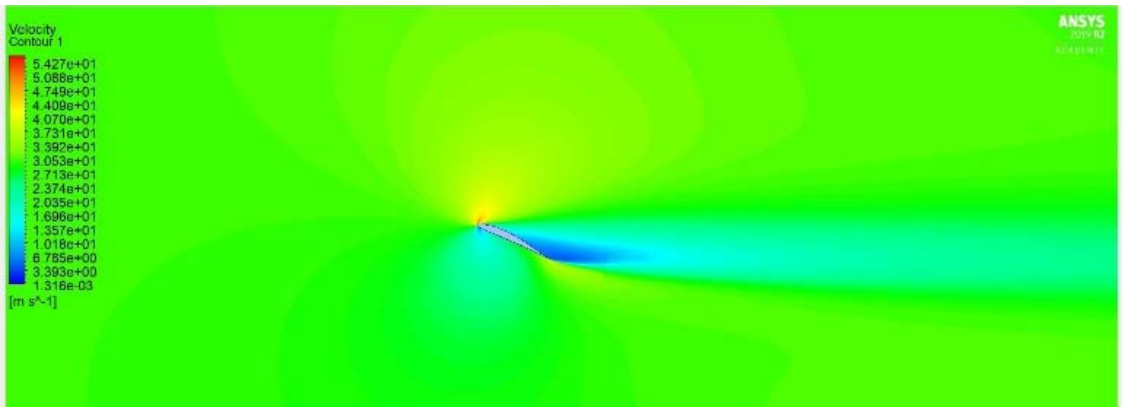

Fig. 7 (b) Velocity Contour of E387 in stall condition

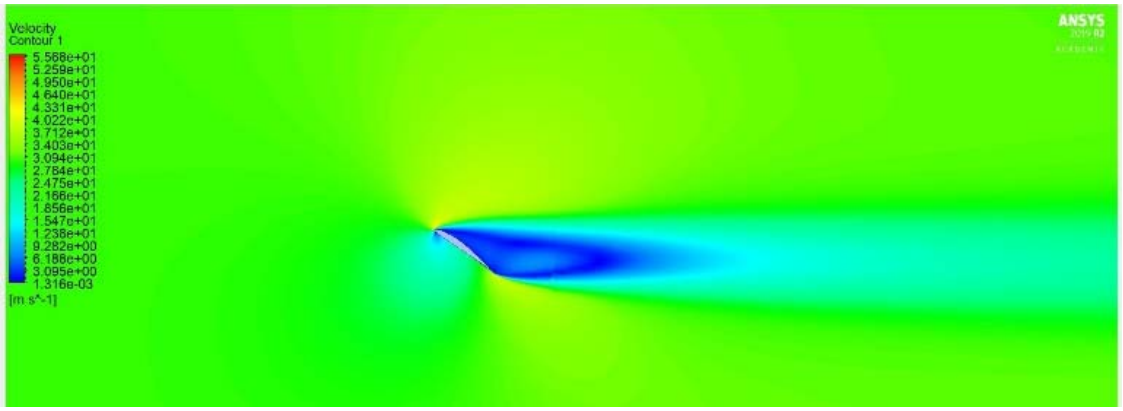

Fig. 7 (c) Velocity Contour of E387 in post-stall condition

B. Selig-Donovan 7003 in Martian and Titan Atmosphere

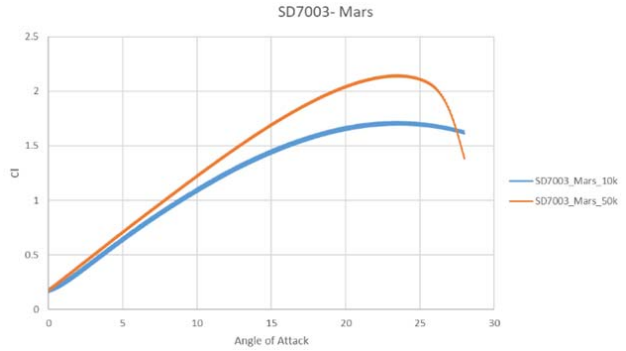

Fig. 8 C_l vs α for SD7003 on Mars at Re = 10000 and Re = 50000 with k = 0.5 rad/s

Fig. 9 C_l vs α for SD7003 on Mars at Re = 10000 and Re= 50000 with k = 0.25 rad/s

TABLE IV
STALL ANGLES ON MARS

SD7003_Mars		
k	Re	Stall angle
0.25	10000	23.84
	50000	20.61
0.5	10000	25.62
	50000	24.55

SD7003 low speed airfoils on Mars at the two different reduced frequencies k = 0.25 rad/s and k = 0.50 rad/s show delayed stall angles at both the Reynolds number. Close similarities can be seen in the behaviors of lift coefficient at the same reduced frequency on Mars. As we can see from the velocity contour in Figs. 12 (a)-(c), during the pre-stall condition there is a higher velocity at the upper surface with formation of proper boundary layer thus resulting in lower pressure. At the stall condition on Mars at Re = 50000 and k = 0.25 rad/s we can see the flow separation region over the surface of the airfoil where the stalling angle is around 20.61 degrees. In the post stall condition, the wake region is formed with turbulences at the rear end of the airfoil.

The stall angles on Martian atmosphere for two reduced frequencies k = 0.25 rad/s and k = 0.5 rad/s are shown in Table IV. It can be observed that the stall angle for both the Reynolds number is similar for respective reduced frequency.

The stall angles on Martian atmosphere for two reduced frequencies k = 0.25 rad/s and k = 0.5 rad/s are shown in Table V. It can be observed that for Re = 50000 the airfoil is stalling much earlier in the Titan atmosphere as compared to the Re = 10000 condition.

TABLE V
STALL ANGLES ON TITAN

SD7003_Titan		
k	Re	Stall angle
0.25	10000	20.83
	50000	9.20
0.5	10000	11.1
	50000	10.47

V. CONCLUSION

The general characteristic of dynamic stall on oscillating airfoil, differences between the light dynamic stall and deep dynamic stall have been explained. This paper has extended the study of dynamic stall in earth's atmosphere to the features of dynamic stall on oscillating airfoils in the Martian and Titan atmosphere. The low Reynolds number airfoil E387 and Selig-Donovan 7003 airfoils are simulated in the atmospheric condition similar to that on mars and titan with different reduced frequency and the experimental results are observed. In the concluding remarks, this study of phenomenon of dynamic stall on Mars and Titan can result in deciding the best

suited airfoil for the UAVs flying in the particular atmospheric condition.

Fig. 10 C_l vs α for SD7003 on Titan at Re = 10000 and Re = 50000 with k = 0.5 rad/s

Fig. 11 C_l vs α for SD7003 on Titan at Re = 10000 and Re = 50000 with k = 0.25 rad/s

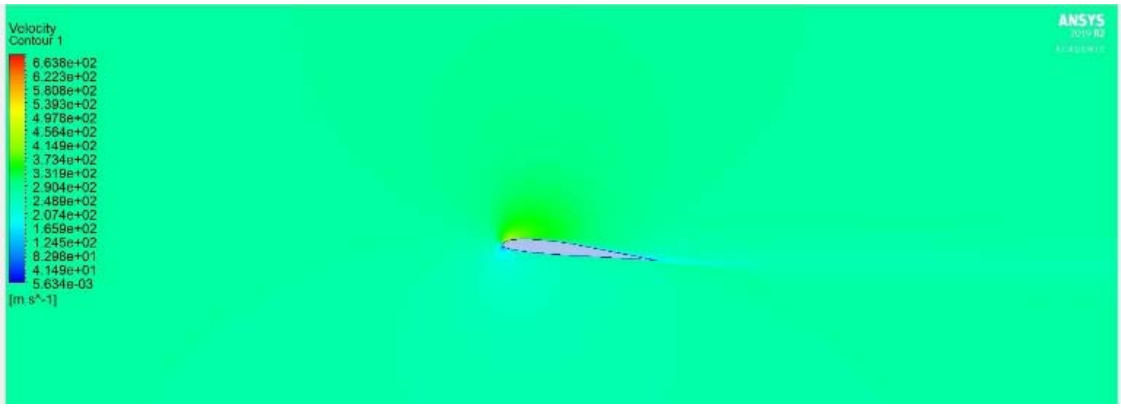

Fig. 12 (a) Velocity Contour of SD7003 in pre-stall

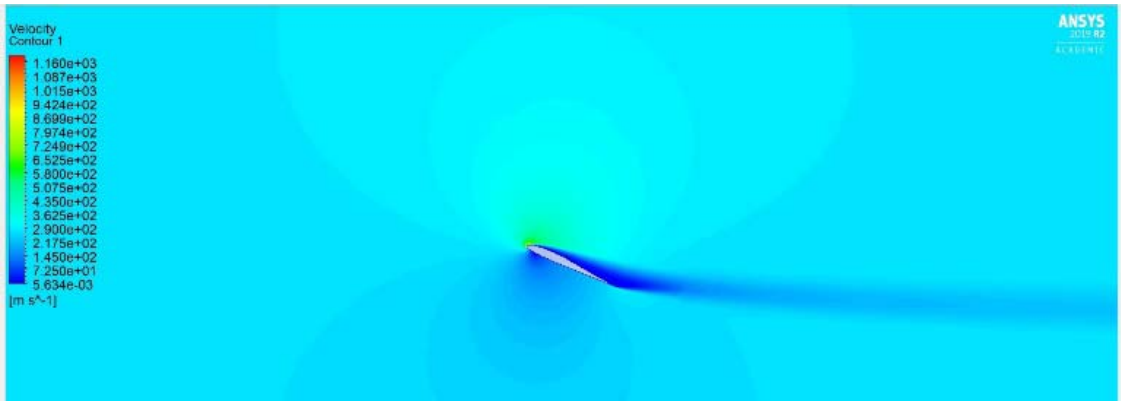

Fig. 12 (b) Velocity Contour of SD7003 in stall

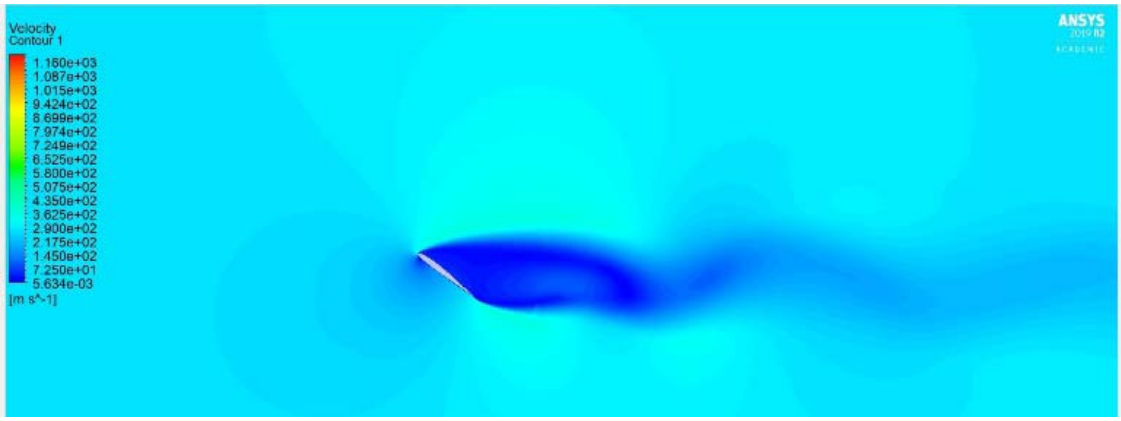

Fig. 12 (c) Velocity Contour of SD7003 in post-stall

REFERENCES

[1] K.W. McAlister, L.W. Carr and W.J. McCroskey, Dynamic Stall Experiments on the NACA 0012 Airfoil, NASA Technical Paper 1100 (January 1978)
[2] B. Petropoulos et C. Macris, Physical parameters of the Martian atmosphere, Earth, Moon, and Planets, Vol.46 (1989), p.1-30
[3] Fundamentals of Aerodynamics, John D. Anderson JR.
[4] Titan as an Exobiotical Environment, A. Coustenis LESIA, Paris-Meudom Observatory, 92195 Meudon, France
[5] W.J. McCroskey, *The phenomenon of dynamic stall*, NASA Technical Memorandum 8126 (1981)
[6] Carr, L. W., "Progress in Analysis and Prediction of Dynamic Stall." Journal of Aircraft, Vol. 25, No. 1, January 1988, pp. 6–17.
[7] K. Mulleners, A. LePape, B. Heine and M. Raffel, *The Dynamics of Static Stall*, 16th Int Symp on Applications of Laser Techniques to Fluid Mechanics Lisbon, Portugal, (09-12 July, 2012).
[8] V. Raghav, N. Komerath and M.J. Smith, *An exploration of the physics of dynamic stall*, ResearchGate (2010)
[9] www.airfoiltools.com